

ATUM-Tomo: A multi-scale approach to cellular ultrastructure by combined volume scanning electron microscopy and electron tomography

Reviewed Preprint

Published from the original preprint after peer review and assessment by eLife.

[About eLife's process](#)

Reviewed preprint posted


October 10, 2023 (this version)

Posted to bioRxiv

August 21, 2023

Sent for peer review

August 21, 2023

Georg Kislinger, Gunar Fabig, Antonia Wehn, Lucia Rodriguez, Hanyi Jiang, Cornelia Niemann, Andrey S. Klymchenko, Nikolaus Plesnila, Thomas Misgeld, Thomas Müller-Reichert, Igor Khalin, Martina Schifferer 

Institute of Neuronal Cell Biology, Technical University Munich, Munich, Germany • German Center for Neurodegenerative Diseases (DZNE), Munich, Germany • Experimental Center, Faculty of Medicine Carl Gustav Carus, Technische Universität Dresden, Dresden, Germany • Institute for Stroke and Dementia Research (ISD), LMU University Hospital, LMU Munich, Germany • Department of Neurosurgery, University of Munich Medical Center, Munich, Germany • Department of Psychiatry and Psychotherapy, University Medicine Greifswald, Greifswald, Germany • Laboratoire de Biophotonique et Pharmacologie, CNRS UMR 7213, Université de Strasbourg, Illkirch, France • Munich Cluster of Systems Neurology (SyNergy), Munich, Germany

 https://en.wikipedia.org/wiki/Open_access

 Copyright information

Abstract

Like other volume electron microscopy approaches, Automated Tape Collecting Ultramicrotomy (ATUM) enables imaging of serial sections deposited on thick plastic tapes by scanning electron microscopy (SEM). However, ATUM is unique by enabling hierarchical imaging and thus efficient screening for target structures as needed e.g., for correlated light and electron microscopy. However, SEM of sections on tape can only access the section surface, thereby limiting the axial resolution to the typical size of cellular vesicles, an order of magnitude lower than the acquired xy resolution. In contrast, serial-section electron tomography (ET), a transmission electron microscopy-based approach, yields isotropic voxels at full EM resolution, but requires deposition of sections on electron-permeant thin and fragile monolayer films – thus making screening of large section libraries difficult and prone to section loss. To combine the strength of both approaches, we developed ‘ATUM-Tomo’, a hybrid method, where sections are first reversibly attached to plastic tape via a dissolvable coating, and after screening detached and transferred to the ET-compatible thin films. Thus, ATUM-SEM of serial semi-thick sections and consecutive ET of one selected section combines SEM’s fast target recognition and coarse rendering capability with ET’s high-resolution volume visualizations – thus enabling multi-scale interrogation of cellular ultrastructure. As a proof-of-principle, we applied correlative ATUM-Tomo to study ultrastructural features of blood brain barrier (BBB) leakiness around microthrombi in a mouse model of traumatic brain injury. Microthrombi and associated sites of BBB leakiness were identified by confocal imaging of injected fluorescent and electron-dense nanoparticles, then relocalized by ATUM-SEM, and finally interrogated by correlated ATUM-Tomo, a workflow which created a seamless zoom-in on structural BBB pathology from the micro- to the nanometer scale. Overall, our new ATUM-Tomo approach will substantially advance ultrastructural analysis of

eLife assessment

This **valuable** methodological development, which combines light (confocal) microscopy with high-resolution scanning EM and EM tomography, expands the level of structural detail accessible to large-volume EM studies and thus represents an approach to integrate the analyses of cellular and sub-cellular levels in biological samples. The data provide a **convincing** proof-of-principle. They will be of particular value to cell biologists interested in the in-depth interpretation of high-resolution ultrastructural information from sparsely distributed targets - at multiple scales and in diverse biological structures.

Introduction

Volume electron microscopy (EM) provides high-resolution data of target structures that can be used to render complex biological morphologies in three dimensions (Peddie et al., 2022). While volume EM thus provides high spatial resolution, searching for a rare nanometer-sized structure of interest in sections of several hundreds of square microns is tedious. To bridge these scale, multimodal approaches like correlative light and electron microscopy (CLEM) (Scher and Avinoam, 2021) or micro-computed tomography combined with volume EM (Karreman et al., 2017) have been applied. Among the available volume EM approaches, array tomography techniques (Wacker and Schroeder, 2013), such as automated tape collecting ultramicrotomy (ATUM) (Kasthuri et al., 2015), have proven particularly powerful for correlating specific biological structures (Schifferer et al., 2021, Snaidero et al., 2020). Array tomography techniques require section collection onto a solid substrate, such as coated glass, silicon (Micheva and Smith, 2007) or plastic tape, and subsequent serial-section scanning electron microscopy (SEM). In ATUM-SEM, a reel-to-reel system transfers the sections from the diamond knife onto tape (Kubota et al., 2018). The tape strips are assembled on a silicon wafer (Baena et al., 2019, Kislinger et al., 2023), thus generating tissue libraries that can be repetitively imaged by SEM at different resolution regimes. This separates the correlation task into two phases: (1) low resolution screening for the region previously imaged by fluorescence microscopy and (2) high resolution volume EM of the target structure.

This high resolution imaging phase of array tomography is, however, currently restricted by physical sectioning, resulting in typical voxels of 3x3x30-100 nm, where SEM determines the lateral resolution of ≈ 3 nm. As a consequence, array tomography can reveal fine cellular processes down to ≈ 40 nm, but potentially misses smaller subcellular structures, such as vesicles or contact sites that can be hidden within a section volume. For higher-resolution imaging typically transmission electron microscopy (TEM) is applied, with electron tomography (ET) being the method of choice for high-resolution volume imaging of small sub-cellular volumes (West et al., 2011, Mastronarde, 2005, He and He, 2014, Kiewisz et al., 2022). In ET, semi-thick sections (200-400 nm) are tilted in the electron beam and Fourier transformed for image reconstruction (Baumeister et al., 1999, Young and Villa, 2023, Frank, 2005), but even with serial semi-thick sections (Soto et al., 1994), the overall volume that can be visualized is limited.

So far, ATUM could not be combined with ET because the former necessitates attaching sections on a solid support, while the latter as a projection method, needs sections to be deposited on electron-transparent films. While conventionally, section deposition is irreversible in ATUM, we reasoned

that plastic tape coating could enable section removal after SEM and transfer onto ET-compatible films. Thus, selected semi-thick sections could be reinspected by ET – a novel multimodal approach, which we call ‘ATUM-Tomo’. We exemplify the ATUM-Tomo approach by assessing structural determinants of blood-brain barrier (BBB) leakiness, a key adaptation of the neurovascular unit that controls substance exchange between blood and central nervous system parenchyma and can be locally disturbed in pathologies, including after ischemia, traumatic brain injury or multiple sclerosis (Zhang et al., 2019 [↗](#), Shi et al., 2020 [↗](#)). We had previously characterized BBB leakage around impact-induced microclots using correlated confocal microscopy and ATUM of fluorescent lipid nanodroplets (LNDs) and gold nanoparticles (Khalin et al., 2022 [↗](#)). At the BBB, the actual barrier function is determined by distinctive ultrastructural features, mostly within the endothelial layer, including tight junctions, pinocytosis and vesicular transport (O’Brown et al., 2019 [↗](#), Andreone et al., 2017 [↗](#), Nahirney et al., 2016 [↗](#), Hirano et al., 1994 [↗](#)). As these structures lie below the 30nm z-resolution limit of ATUM, they eluded our previous correlative imaging – but we now demonstrate that triple correlation using confocal microscopy, volume SEM and ET can provide an integrated view of the cellular environment as well as the ultrastructural features of the compromised BBB. This application demonstrates that ATUM-Tomo in combination with CLEM is a powerful multimodal approach, enabling a bridging of scales from the mm to nm range.

Results

Correlated confocal imaging and ATUM-SEM reveals sites of BBB disruption

Controlled cortical impact in mice is a model for traumatic brain injury that involves BBB damage. To mark sites of vessel injury, we injected LNDs and colloidal gold particles of similar size (30nm) and surface chemistry (PEGylation) ensuring similar biodistribution. LNDs are highly fluorescent, while gold is electron dense – and both accumulate in microthrombi formed in the impact penumbra within 30-60 min post-injection (Khalin et al., 2022 [↗](#)) enabling the tracking of microthrombi and BBB leakage sites. These particles were injected systemically 60 min after impact, followed by DyLight 649 lectin as a vessel lumen marker just before perfusion with fixative containing glutaraldehyde, which all fluorophores withstand (Fig. 1A [↗](#)). We sliced the fixed brains in 80 µm thick coronal vibratome sections (Fig. 1A [↗](#)) to allow confocal imaging and preserve some longer stretches of blood vessels, while restricting the axial depth of the search volume for correlation. After post-fixation in glutaraldehyde, sections were temporarily mounted on a glass slide with a cover slip and recorded ~2x2 mm confocal overview of all cortical layers bearing the lesion and perilesion areas (Fig. 1B [↗](#)). For correlative EM, we identified areas of vascular occlusions indicated by LNDs accumulations and sites of extravasation marked by perivascular LND fluorescence and locally acquired higher magnification confocal image stacks (Fig. 1B [↗](#)). Tissue preservation was ensured by imaging for a maximum of one hour, followed by gentle removal of the cover slip by floating-off in buffer.

In order to keep the section flat during EM processing and to minimize the search volume, we dissected the smallest possible tissue block around the region of interest based on tissue fiducials as a guide. The tissue was processed for EM by a standard reduced-osmium-thiocarbohydrazide-osmium (rOTO) *en bloc* staining protocol (Hua et al., 2015 [↗](#)) in a way that facilitates the axial and lateral relocation of the area of interest (Kislinger et al., 2020a [↗](#)). Production of serial thin (100 nm) sections and collection of these sections on either carbon-coated Kapton (ccKapton) (Kasthuri et al., 2015 [↗](#)) or carbon nanotube (Kubota et al., 2018 [↗](#)) tape generated a library of ribbons. A typical 1000 section library was collected, which could then be imaged hierarchically and repetitively. For an overview to facilitate correlation, we imaged the entire area of every 10th

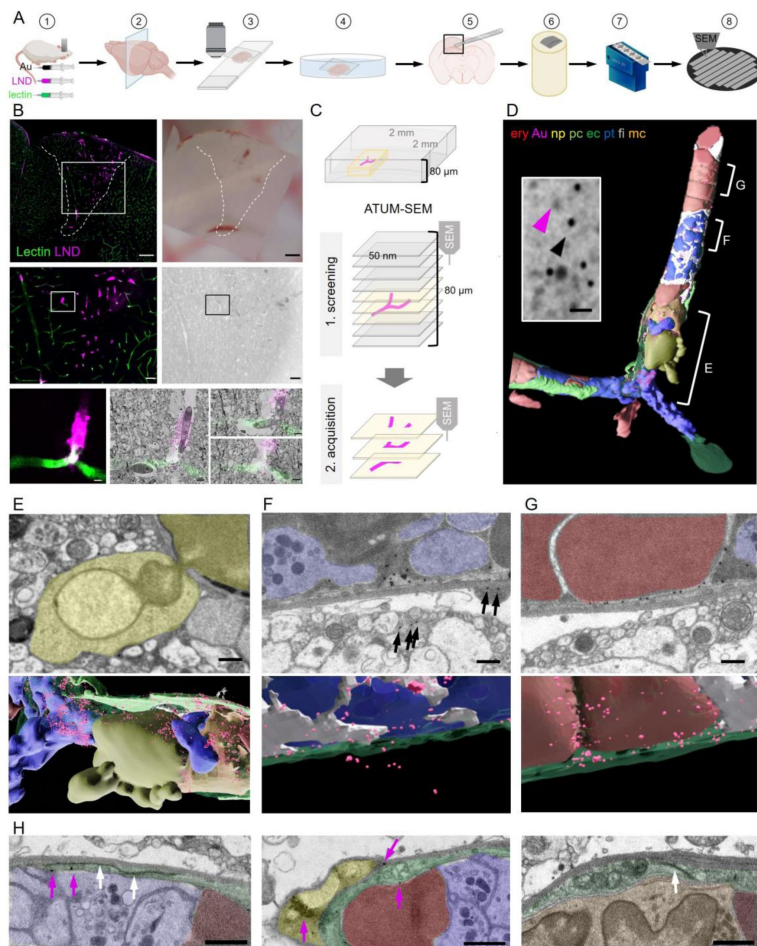


Figure 1.

Correlative confocal microscopy and ATUM-SEM reveals hallmarks of vascular occlusions and extravasation. **(A)** Schematic drawing of the ATUM-SEM CLEM workflow. Controlled cortical impact (middle) is followed by systemic injection of 30 nm diameter LNDs (magenta) and 30 nm diameter colloidal gold nanoparticles (black). DyLight 649 lectin (green) was injected 5 min before perfusion (1). After fixation, coronal vibratome sections are generated (2) and positioned onto glass slides with only laying the cover slip on top of the section for confocal imaging (3). The vibratome section is recovered by immersion into the petri dish (4). The previously imaged region of interest is dissected (5) and processed for EM including embedding into resin and contrast enhancement (6). Serial ultramicrotomy and tape collection (7) is followed by wafer mounting and SEM imaging (8). **(B)** Top: Sum projection of a confocal tile scan (lectin, green; LNDs, magenta; left) and corresponding binocular image (right) of the dissected vibratome section. The lesion area is indicated by a dashed line. Scale bar, 200 μ m. Middle: Lesion area identified in the overview tile scan (box in top image) is relocated in the sum projection confocal image and in the serial section low resolution SEM (right). Scale bar, 50 μ m. The region of interest (ROI, box) is chosen in the confocal image and re-located in the sum projection SEM image. Bottom: Region of interest confocal image (left) and three single SEM micrographs overlaid with the correlated confocal images (right). Scale bar 5 μ m. **(C)** Scheme of the ATUM-SEM strategy for CLEM. A blood vessel of interest (magenta) in an 80 μ m thick vibratome section is relocated by screening serial ultrathin sections at low resolution. The target region is reimaged at high resolution (up to 5x5x50 nm). **(D)** The correlated region in **(B)** was segmented and reconstructed from the ultrastructural data. Endothelium (ec, dark green), LNDs and gold particles (Au, magenta), monocyte (mc, orange), neutrophil (np, yellow), platelet (pt, blue), fibrin (fi, grey), erythrocytes (ery, red), pericyte (pc, bright green) are shown. Inset: SEM image of vessel lumen filled with equally sized, putative LNDs (magenta arrowhead) and gold particles (black arrowhead) and bigger aggregates thereof. Scale bar, 100 nm. **(E-G)** Segmented SEM image (top) and three-dimensional rendering thereof (bottom), scale bars 1 μ m, showing **(E)** the extravasation site from of a neutrophil (yellow), **(F)** extraluminal gold particles (arrows) next to vessel lumen clotted with platelets (blue) and fibrin (grey) and **(G)** stalled erythrocytes (red) interspersed with colloidal gold particles. **(H)** Endothelial morphologies from left to right: normal endothelium (dark green) with tight junction (white arrows) and gold particles (magenta arrows); thinned endothelium covered by a pericyte (bright green), swollen endothelium with mitochondria and tight junction. Immune cells (orange), erythrocytes (red), platelets (blue). Scale bars 1 μ m.

section (i.e. 1000 nm axial sampling) with 200x200nm lateral sampling. This allowed us to efficiently screen such a serial-section library for regions of interest, even if the confocal imaging and ultramicrotomy planes were not perfectly aligned.

Regions with microthrombi and extravasation were identified by correlation and selected for high-resolution (4x4x100 nm) data acquisition by volume SEM. Microthrombi were characterized by a high LND signal, while, sites of extravasation showed a perivascular halo. The microclot illustrated here consisted of luminal erythrocyte stalls (**Fig. 1D,G**) in combination with platelets and immune cells (**Fig. 1D,H**). An accumulation of platelets, interspersed with filamentous, electron-dense fibrin was found in the center and at the ends, “plugging” the occlusion (**Fig. 1D,F,H**). Correlating to the fluorescence pattern, we detected gold particles and brighter but less discrete particles of the same size, presumably representing LNDs, between luminal cells (**Fig. 1D**). Healthy endothelium was characterized by an intact glycocalyx and hence lectin staining in the absence of LND fluorescence. In contrast, at a sites of extravasation indicated by an LND halo, we found a neutrophil undergoing diapedesis (**Fig. 1E**) and abluminal gold particles (**Fig. 1F**). Thus, we can assume that some microthrombi could serve not only as an entry points for nanoparticles, but also for cells from blood. Within the microthrombus periphery, regions of the endothelium were swollen with intact tight junctions, while in the core, regions with almost no discrete endothelial layer prevailed (**Fig.1H**). Colloidal gold was found at pathologically thinned endothelium, basement membrane and in pericytes (**Fig. 1F-H**).

Development of reversible section attachment on coated tape for ATUM-Tomo

ATUM-SEM revealed the cellular composition of vascular occlusions and ultrastructural features of BBB leakiness. While transcellular or paracellular pathways are supposed to be involved, so far, early transport mechanisms have not been fully understood. The existence of morphological normal tight junctions visualized by ATUM-SEM suggests that vesicular transport might be involved. However, resolving gold-particle loaded vesicles at 20-40 nm diameter or tight junctions challenges the axial resolution of ATUM-SEM (≈ 30 nm). Therefore, we sought to combine ATUM-SEM and ET, as the latter would provide the required resolution ([Michel, 2012](#), [Feng et al., 2002](#), [Wagner et al., 2012](#)), but the former would allow efficient screening across an expanded field of view ([Peddie et al., 2022](#)). For this purpose, we devised a new method to reversibly attach semi-thick ATUM sections to plastic tape for SEM and then transfer them to TEM grids for ET.

We first tested if conventionally collected sections of mouse cortical tissue can be removed from ccKapton or carbon nanotube tape. However, such sections were stuck to the tape despite treatment with organic solvents and any other chemical or physical treatments that we tested (**Fig. 2A**). We then hypothesized that adding a thin, dissolvable coating between tape and section could allow gentle detachment (**Fig. 2B,C**). Polyvinyl formal (Formvar) was a good candidate, as thin films of this highly solvable polymer are commonly used to support TEM sections. Moreover, it has been shown that sections can be transferred from Formvar-coated glass coverslips onto TEM grids by hydrofluoric acid ([Paez-Segala et al., 2015](#)). Therefore, we tested if an ultrathin tissue section could be removed from Formvar-coated tape by organic solvents. Short ccKapton tape strips were Formvar-coated using a standard film casting device (cfcKapton), onto which 100-300 nm tissue sections were collected from the diamond knife water bath. Indeed, such sections could be recovered from the tape by incubation in chloroform or 1,2-dichloroethane. To coat longer stretches of tape, we designed a reel-to-reel coating device with a spraying unit (Suppl. Fig. 1). We mounted such longer cfcKapton tape with tissue sections onto wafers, as required for ATUM-SEM, and subjected them to SEM imaging. We found that Formvar coating induced charging, depending on the thickness of the coat (**Fig. 2D**). In addition, imaging at high resolution (<10 nm) prevented subsequent section detachment (Suppl. Fig. 2).

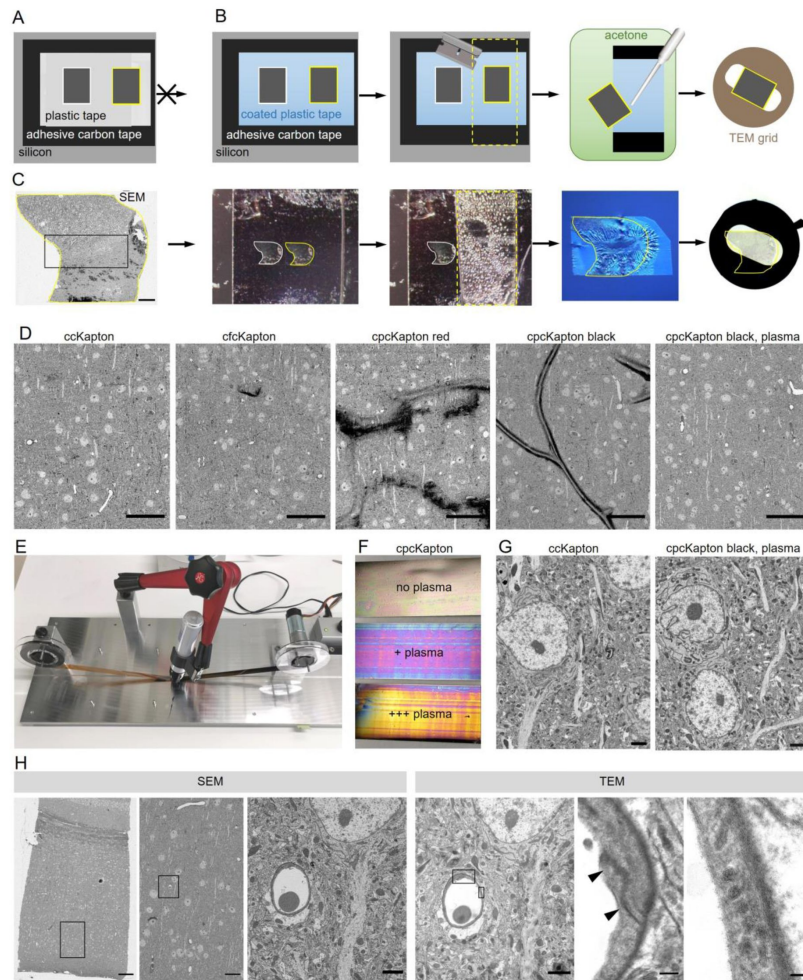


Figure 2.

with 4 supplements. Principle of reversible section attachment on coated tape. **(A)** Schematic showing that sections on ccKapton mounted on a silicon wafer cannot be recovered for TEM. **(B)** Schematics of section removal from cpcKapton or cfcKapton. From left to right: The adhesive tape around the selected section (yellow border) is excised by a razor blade (cutting line: yellow dashed lines) and detached from the wafer. The section is detached from the tape by acetone rinsing using a pipette. The section is collected from the acetone bath onto a TEM slot grid. **(C)** Detachment workflow of a particular selected section (yellow border). From left to right: SEM overview image of a section (scale bar 200 nm); the imaged section mounted on the wafer; the section is removed together with the underlying adhesive tape (cutting line: yellow dashed lines); the section is floating on a water bath of a diamond knife after acetone treatment; slot grid with the section. **(D)** SEM images of mouse cortex specimens collected onto different Kapton tapes. From left to right: ccKapton; cfcKapton showing a charging artifact (arrow); cpcKapton red with major charging; cpcKapton black without plasma treatment showing section folds; cpcKapton black after intense plasma treatment. Scale bars 50 μm . **(E)** Photograph of the coating unit with a permanent pen and halfway labelled ccKapton. **(F)** Photograph of cpcKapton before discharging (top), after mild (middle) and extensive (bottom) plasma discharging. **(G)** Ultrastructural quality of a cortical tissue section on ccKapton (left) and cpcKapton after plasma treatment (right) imaged at 10x10 nm resolution. Scale bars, 2 μm . **(H)** Recovery of an ultrathin section. From left to right: SEM overview image of cortex with corpus callosum (scale bar 100 μm). SEM medium resolution image thereof (scale bar, 10 μm). SEM high-resolution image (10 x 10 nm) of a blood vessel cross section (scale bar, 2 μm). TEM image of the same section showing the selected blood vessel (scale bar, 2 μm). High magnification image of a tight junction (arrowheads), scale bar 200 nm. High magnification images of endothelial vesicles (scale bar, 50 nm). Black boxes indicate location of the image to the right. The online version of this article includes the following figure supplements for **figure 3** [↗](#):

Figure supplement 1. Formvar coating for reversible section collection.

Figure supplement 2. Optimizing SEM imaging conditions for section detachment.

Figure supplement 3. Contamination of section surface after detachment.

Figure supplement 4. Estimation of distortion between SEM and TEM images.

In order to avoid these problems we considered other material that are soluble in organic solvents, and settled on the simple and readily available solution of permanent markers (edding International GmbH). Edding marker pens consist of genuine pigmented alcohol-based ink and humectants while a special resin ensures that it is waterproof. We labeled ccKapton with a thin film of permanent marker with wide tip (cpcKapton) and found that sections attached to such tape could be detached by intense rinsing with acetone. The resulting floating sections could be transferred to a water bath in a drop of acetone using a single-use Pasteur pipette. For longer stretches of tape as needed for serial sections, we rededicated the coating unit by installation of a permanent marker instead of the spraying unit (**Fig. 2E** [↗](#)).

Next, we assessed the SEM imaging characteristics of tissue sections on cpcKapton mounted on silicon wafers. Coatings with permanent marker of red color, but not black color partially detached from the plastic support and lead to strong charging during SEM imaging (**Fig. 2D** [↗](#)). Tissue sections attached to cpcKapton, using pens of either color, showed major tissue section folds (**Fig. 2D** [↗](#)). In order to remove these folds, we plasma discharged black cpcKapton tape extensively (see Material and Methods) until the film interference color changed from black to magenta (mild discharging) to gold (extensive discharging) (**Fig. 2F** [↗](#)). Such plasma-discharged cpcKapton enabled reversible section attachment at certain SEM imaging conditions (10 nm lateral resolution at 3 μ s dwell time) with ultrastructural quality comparable to ccKapton (**Fig. 2G** [↗](#)).

We then assessed the tissue ultrastructure in the TEM and the possibility to relocate regions previously imaged by SEM. For this purpose, 80 nm sections on cpcKapton were wafer-mounted, imaged by SEM and transferred to TEM grids. Despite extensive acetone rinsing the sections stayed intact with well-preserved ultrastructure. The *en bloc* embedding provided strong TEM image contrast without further poststaining. If the section area exceeds the slot size, we deposited the region of interest at the grid center. We could efficiently relocate the previously SEM-imaged region in the TEM by using tissue-intrinsic fiducials at low resolution (**Fig. 2H** [↗](#)). However, we detected dark deposits (Suppl. Fig. 3A) on some regions of the section, which probably originate from tissue contact with the coating and accordingly are only superficial. As ET that mainly visualizes the inner tissue areas of the semi-thick sections, we considered these deposits as unproblematic, and cpcKapton hence as a potentially suitable support material for combining ATUM-SEM and ET to bridge across scales (**Fig. 3A, B** [↗](#)), which we probed by applying this approach to assess BBB integrity after traumatic brain injury.

ATUM-CLEM and ATUM-Tomo of nanoparticles at the leaky BBB

To this end, confocal imaging and EM processing of a traumatic brain injury lesion were performed as described for correlative ATUM-SEM. We collected serial 400 nm-thick sections of the lesion area covering the entire volume of the vibratome section on cpcKapton. Typically, this resulted in 250 sections that can be mounted onto one or two wafers, dramatically speeding up the correlation process compared to ATUM-SEM (1000 sections on four wafers). We imaged the entire section areas at 100 nm lateral resolution to screen for rough anatomical landmarks. Two vessels with high LND fluorescence signal (**Fig. 3C** [↗](#)) were correlated and selected for imaging at higher resolution (20x20 nm). Based on this ultrastructural volume and in order to unambiguously identify the localization of nanoparticles, we acquired single images of these target regions at 10 nm lateral resolution. Alignment and three-dimensional rendering of the volume EM data (**Fig. 3D** [↗](#)) provided an overview of the underlying neurovascular unit despite the coarser axial resolution compared to ATUM-SEM. Based on these reconstructions and inspection of the ultrastructural volume, we selected sections with gold particles potentially crossing the BBB. These tissue sections were detached by acetone treatment and collected onto Formvar-coated slot grids, as needed for subsequent ET. We found that colloidal gold fiducials (20 nm diameter) needed for image reconstruction could be attached to the surface of these sections despite previous SEM imaging. Tomographic reconstructions of semi-thick sections removed from cpcKapton showed surface contamination only at the side that was facing the permanent marker coat penetrating

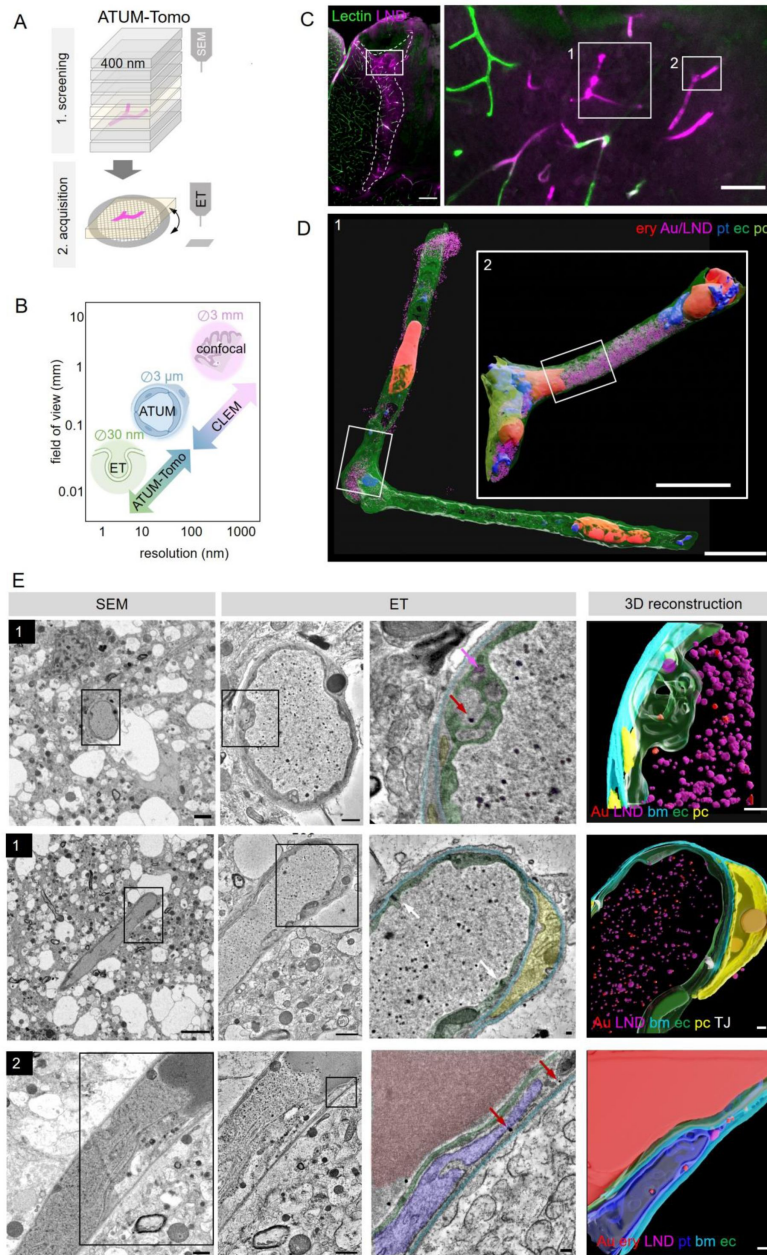


Fig. 3.

Correlated ATUM-Tomo of vascular occlusions. **(A)** Schematic of the ATUM-Tomo workflow. Semi-thick sections are serially imaged by SEM. Targeted sections (yellow) bearing the site of interest (blood vessel, magenta) are selected for ET. **(B)** Schematic highlighting how ATUM-Tomo and CLEM-ATUM-Tomo bridge scales in resolution and field of view. TEM-tomography enables high resolution e.g. for vesicular structures (diameter ~30 nm), ATUM the cellular composition and morphology (e.g. neurovascular unit) (diameter ~30 nm) and confocal provides a large field of view (e.g. highlighting a lesion site in cortex, 3x3 mm). **(C)** Confocal microscopy images of the traumatic brain injury lesion. Lectin (green), LNDs (magenta). Numbered boxes indicate positions selected for SEM imaging. Scale bars 200 μ m, 20 μ m. **(D)** Reconstruction of selected vessels as indicated in (C). Scale bar 10 μ m. **(E)** Regions from the vessels 1 (first two rows) and 2 (third row) in (D) selected for ET. SEM image (first column, scale bar 2 μ m first and, third row; 5 μ m second row), corresponding ET low (second column, scale bar 500 nm) and high magnification images with segmentation (third column, scale bar 100 nm) and three-dimensional reconstruction thereof (fourth column, scale bar 200 nm). First row: Example of particles in endothelial swellings (red arrow gold particle, magenta arrow LND). Second row: Intact tight junctions (white arrow). Third row: Endothelial disruption and gold particle localization in a platelet. Endothelium (green), pericyte (yellow), platelet (blue), basement membrane (cyan), LNDs (magenta), gold nanoparticles (red), tight junctions (white).

down to a depth of up to 50 nm into the section (Suppl. Fig. 3B). Sections that were collected at a nominal cutting thickness of 400 nm showed an actual thickness of 260-300 nm after the tomographic reconstruction. This collapse is due to a mass loss after interaction of the electron beam with the specimen (Luther et al., 1988 [↗](#), McEwen and Marko, 1998 [↗](#), O'Toole et al., 2020 [↗](#)). Moreover, we detected variable tissue shrinkage laterally of about 20% and minor distortions between the SEM and TEM images of ultrathin sections, probably due to beam damage and acetone treatment (Suppl. Fig. 4).

Despite these minor changes, the features of the targeted microthrombi and the surrounding neurovascular unit familiar from conventional thin-sectioning ATUM-SEM could be readily discerned: The unit's cellular layers with endothelial cells, basement membrane and pericytic processes could be visualized, even at pathological sites. Moreover, the injected colloidal gold particles and LNDs were accumulated in the vessel lumen, with the identification of LNDs — compared to SEM images—actually facilitated in the ET by the increased resolution (Fig. 3E [↗](#)). We observed that the endothelial layer showed local edema and detachment from the basement membrane, while tight junctions were still intact (Fig. 3E [↗](#)). Gold particles were detected in platelet vesicles, vacuoles of endothelial cell swellings, as well as in areas of endothelial detachment from the basement membrane (Fig. 3E [↗](#)). We also recovered and reconstructed tomograms from nine serial semi-thick sections (Fig. 4 [↗](#)). Comparing the SEM reconstruction with the one from the corresponding serial ETs clearly shows that SEM imaging visualizes only the section surface resulting in a coarse three-dimensional rendering, while ET provides information of the entire section thickness (Fig. 4B-D [↗](#)). Taken together, this correlated ATUM-Tomo approach enabled the targeted visualization of extravasating nanoparticles and their ultrastructural organelle carriers within reconstructed CNS neuropil contextualized by confocal and volume SEM imaging – a valuable approach to bridge from micro-to nanoscales in the electron microscopic examination of healthy and diseased tissue samples.

Discussion

We and others have shown previously that non-destructive array tomography -type volume EM methods like ATUM-SEM are particularly powerful for correlative workflows, because tissue libraries with reimaging capabilities are generated (Schifferer et al., 2021 [↗](#)). In contrast, destructive block-face volume EM methods only allow a single shot acquisition and are limited in field of view. The ATUM imaging process can be separated into screening at low resolution for the sites of interest and subsequent high-resolution volume acquisition. ATUM-SEM allows the rendering of cellular and organellar morphologies at the ultrastructural level. However, the visualization of the detailed subcellular environment of nanoscale structures is limited to the maximal lateral resolution achievable by SEM and the axial resolution set by physical section thickness (30 nm). To increase the axial resolution of target structures we previously combined ATUM with Focused Ion Beam (FIB) milling. ATUM-FIB takes advantage of semi-thick section (2-10 μm) imaging for screening combined with FIB-SEM acquisition of the target region at isotropic voxels (Kislinger et al., 2020a [↗](#), Kislinger et al., 2020b [↗](#)). While ATUM-FIB enables targeted volume imaging at 3x3x3 nm resolution. The only room temperature volume EM methods that can provide higher resolution are serial section TEM or ET (Peddie et al., 2022 [↗](#), Schneider et al., 2021 [↗](#)). While serial-section ET has proven suitable to resolve and reconstruct volumes of abundant biological targets (Soto et al., 1994 [↗](#), Rachel et al., Horstmann et al., 2012 [↗](#)), the visualization of rare or correlated structures is tedious and time consuming. So far, automated serial TEM can only be done by collection of serial ultrathin sections onto grid tape, a plastic tape with holes covered with a thin support film at defined distances (Graham et al., 2019 [↗](#)). Besides high costs for the tape, the ultramicrotome has to be automatized to make sure that the section is positioned onto the slot and not the grid bar. Moreover, a standard TEM has to be redesigned for a reel-to-reel sample loading system (Maniates-Selvin et al., 2020 [↗](#), Yin et al., 2020 [↗](#)), which is not compatible with ET and obviates its application in a standard EM facility.

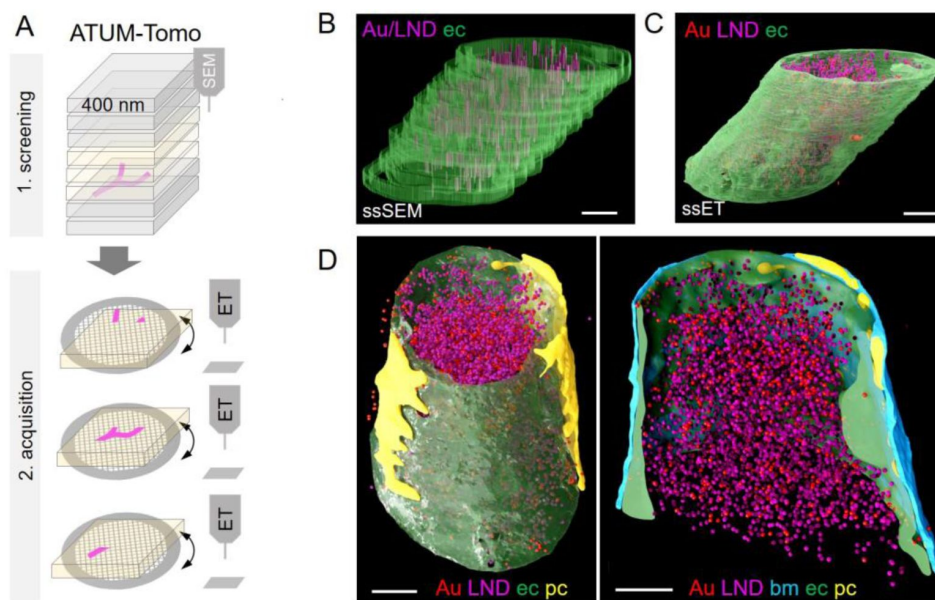


Fig. 4.

Correlated ATUM-Tomo with serial section ET. **(A)** Schematic of the ATUM-Tomo workflow. Semi-thick sections are serially imaged by SEM. Targeted sections (yellow) bearing the site of interest (blood vessel, magenta) are selected for serial section ET. Tomograms from consecutive ET volumes can be aligned. **(B-D)** The boxed region in **Fig. 3** [D](#) (number 2) has been subjected to ET of nine consecutive sections. (Endothelium (green), pericyte (yellow), platelet (blue), basement membrane (cyan), LNDs (magenta), gold nanoparticles (red)). Scale bars 1 μm . **(B)** Non-smoothed, raw reconstructions of nine consecutive SEM images. **(C)** Corresponding region of nine detached sections subjected to ET and reconstructed. **(D)** Side view (left) and longitudinal cut view (right) of the smoothed serial section ET reconstruction.

Our novel ATUM-Tomo approach provides a simple and inexpensive way of combining large volume SEM with targeted TEM at isotropic, high-resolution voxels. As TEM is a projection method, it requires the removal of the solid substrate, which is needed for SEM imaging. Here we developed a simple tape coating technique that allows consecutive section inspection by the two EM modalities. Formvar coating resulted in reversible section collection but heterogeneity in film thickness led to charging artefacts, background signal and sites of irreversible section attachment. We found that marker pen coating provided a simple, reproducible and homogenous coating. Using pen-coated tape, we were able to image hierarchically up to a lateral resolution of 10 nm by SEM, while retaining the recovery option for transfer onto grids. Detachment of semi-thick sections by acetone did not result in major section distortion. The detachment of ultrathin sections proved more difficult due to section folding and fragility during acetone rinsing. Moreover, surface contaminations might potentially cover sites of interest which has more pronounced consequences for the information content of ultrathin than semi-thick sections. Surprisingly, previous SEM imaging does not affect the ultrastructural quality of the ET images. Section folds usually occur at sites within the tissue that have not been imaged by SEM before. This might be caused by reinforced section attachment to the tape caused by prolonged exposure to the electron beam. This effect is even beneficial as it guides the positioning of tissue sections onto the TEM grid slot if it exceeds its area. The SEM volume reconstructed from serial semi-thick sections shows a coarser morphology compared to serial ultrathin sections but still provides the information needed for the selection of sections to be subjected to ET. There was minor tissue loss between consecutive tomograms. This was probably caused by a combination of standard material loss through sectioning (Hayworth et al., 2015 [↗](#), Kislinger et al., 2020b [↗](#)) and the missing cone due to incomplete tomographic information from high tilt angles (Barth et al., 1988 [↗](#), Ding et al., 2019 [↗](#)) (Suppl. Fig. 3, **Fig. 4B** [↗](#)). While we observed tissue loss due to surface contaminations and sectioning, we were able to recover and reconstruct a volume of up to nine consecutive semi-thick sections by ET. Thus, we demonstrate that *en bloc* stained tissue can be sequentially imaged by volume SEM and ET at high ultrastructural quality.

We inspected microthrombi in traumatic brain injury by both correlated ATUM and ATUM-Tomo. In both cases, CLEM was facilitated by preservation of lectin and LND fluorescence despite glutaraldehyde fixation, a prerequisite for optimal ultrastructural preservation. While LNDs enable the detection of microthrombi and sites of BBB leakage by confocal microscopy, their size and contrast show variability in SEM and TEM micrographs. Here, detection of abluminal gold particles served as a clear indicator of extravasation by virtue of high electron density and discrete size of the gold particles. Nanoparticles were found among luminal cells and close to sites of immune cell diapedesis. By virtue of the novel ATUM-Tomo approach, we captured nanoparticles at sites of endothelial swellings. In line with our results, earlier studies already described endothelial edema preceding FITC-albumin early after middle cerebral artery occlusion (Krueger et al., 2015 [↗](#), Krueger et al., 2019 [↗](#)), another model system for studying BBB leakiness. At later stages, these authors observed loss of endothelial cell integrity with discontinuous plasma membranes and detachment from the basement membrane. However, the DAB staining of FITC-albumin applied in these studies masks the endothelial ultrastructure and thus provide compromised EM information (Krueger et al., 2019 [↗](#)). In contrast, our CLEM approach provides high ultrastructural quality by optimal chemical fixation. Endothelial swellings were identified at regions without lectin staining, only showing LND fluorescence. Lectin serves as a marker for intact glycocalyx and its loss indicates early pathological events leading to activation of transcellular transport. It was shown that the glycocalyx is critical for BBB integrity by suppressing caveolin1-dependent endothelial transcytosis following ischemic stroke (Zhu et al., 2022 [↗](#)). This is in line with the detection of intact tight junctions and gold particles in vesicles at sites of BBB leakiness in the current and previous studies (Krueger et al., 2015 [↗](#)). In contrast, the paracellular pathway seems not to be the first loophole and gains importance starting 48 h after the injury (Knowland et al., 2014 [↗](#)).

In summary, we developed a simple and low-cost method for multimodal EM imaging that combines the strengths of both volume SEM and ET. Our novel ATUM-Tomo approach enables the consecutive inspection of selected areas of interest by correlated serial SEM and TEM, optionally in combination with CLEM. ATUM-Tomo and particularly correlative ATUM-Tomo can bridge several scales, which is particularly important for ultrastructural analysis of focal pathologies or rare cellular and subcellular events. Both imaging modalities are non-destructive, thus allowing re-imaging and hierarchical imaging at the SEM and TEM levels, which is especially important for precious samples including human biopsies and complex CLEM experiments. While we demonstrate a neuropathology-related application, further biological targets that require high-resolution isotropic voxels include the detection of gap junctions for connectomics (Holler et al., 2021 [↗](#)) and the subcellular location of virus particles (Wu et al., 2022 [↗](#), Roingeard, 2008 [↗](#), Pelchen-Matthews and Marsh, 2007 [↗](#)). Thus, ATUM-Tomo opens up new possibilities in multimodal volume EM imaging for diverse biological areas of research.

Material and Methods

Controlled cortical impact model of traumatic brain injury

All animal experiments were approved by the Ethical Review Board of the Government of Upper Bavaria. The data were collected in accordance with the ARRIVE guidelines (Kilkenny et al., 2010 [↗](#)) recommendations (Guillen, 2012 [↗](#)). Animal husbandry, health screens, and hygiene management checks were performed in accordance with Federation of European Laboratory Animal Science Associations (FELASA) guidelines and recommendations. 12 C57Bl/6N male mice, 23–25 g, underwent controlled cortical impact as described above and our in previous studies (Wehn et al., 2021 [↗](#)).

This model induces a highly reproducible lesion that shares many characteristics of human traumatic brain injury. In short, after induction of anesthesia with buprenorphine (100 mg kg⁻¹ Bw) and isoflurane (4%, 30s), animals were sedated with 1.5–2.5% isoflurane in oxygen/air under continuous monitoring of body temperature and heart rate. After right parietal craniotomy, the impact is directly applied to the intact dura with a pressure-controlled custom made controlled cortical impact device (L. Kopacz, University of Mainz, Germany; 6 m s⁻¹, 0.5 mm penetration depth, 150 ms contact time). After re-fixation of the skull plate and surgical closure, animals are ventilated with 100% oxygen until they regained consciousness, then were kept in an incubator at 34 °C and 60% humidity in order to prevent hypothermia. Perfusion, confocal imaging and correlated ATUM-SEM were performed as previously described (Khalin et al., 2022 [↗](#)).

Lipid nanodroplets

Dye-loaded lipid nanoemulsions droplets were produced by spontaneous nanoemulsification by adapting previously described protocols (Bouchaala et al., 2016 [↗](#)). Briefly, the 1% solution of R18/TPB (prepared as described earlier (Reisch et al., 2014 [↗](#))) in LabrafacWL® was mixed with Kolliphor ELP®, and the mixture was homogenized under magnetic stirring at 37 °C for 10 min. The amounts of LabrafacWL® and Kolliphor ELP® were 40 and 60 mg, respectively. Finally, LNDs were obtained by addition of 230 mg Milli-Q water. Hydrodynamic diameter was measured by dynamic light scattering (DLS) using a Zetasizer Nano ZSP (Malvern Instruments S.A., Worcestershire, UK), based on volume statistics.

Injection

For injection of lectin and NPs we used an established femoral arterial catheterization protocol (Khalin et al., 2020 [↗](#)). 1 mg/ml DyLight 649 Labeled Lycopersicon Esculentum (Tomato) Lectin (Vector Laboratories, Burlingame, CA, US) for labelling of blood vessels was injected in a quantity of 0.1 ml per mouse. Commercially available 30 nm colloidal gold nanoparticles with density 1.00

g/cm³, methyl terminated, PEG 2000 coated (Sigma-Aldrich, St. Louis, Missouri, USA) were injected through femoral catheter into the mouse in the same dose as LNDs (4 µL/g animal) (Khalin et al., 2022 [DOI](#)). LNDs were formulated using the nano-emulsification approach, as was described (Khalin et al., 2022 [DOI](#)). Hydrodynamic diameter and polydispersity were measured by DLS using a Zetasizer Nano ZSP (Malvern Instruments S.A., Worcestershire, UK), using volume statistics. The size of LNDs was 35.66±1.66 nm, PDI index 0.113±0.002.

Tissue collection

Animals were transcardially perfused with 4% PFA and 2.5% glutaraldehyde in PBS pH 7.4 in deep anesthesia. The brain was collected and the lesion area of fixed brains was subsequently cut in vibratome in rostral-caudal direction into 80-100 µm sections using a vibratome as previously described (Ghosh et al., 2015 [DOI](#)). In order to ensure high ultrastructural preservation, sections were postfixed in the same fixative and carefully transferred using brushes. Instead of standard mounting which could harm the tissue, sections were mounted onto a glass slide using mounting medium (Aqueous Mounting Medium (ab128982), Abcam, Cambridge, UK) diluted with PBS at a ratio of 1:5. A cover slip (0.17 µm, Menzel Gläser, Braunschweig, Germany) was then placed onto it for imaging. After performing confocal microscopy, the mounted sections were submerged in PBS and the cover slip carefully removed. Sections could then be transferred back into 24-well plates with fresh buffer for further processing.

Confocal imaging for correlation

Imaging was performed using confocal microscopy (ZEISS LSM 900, Carl Zeiss Microscopy GmbH, Jena Germany). Confocal imaging revealed that lectin and LND fluorescence was possible with minimal autofluorescence despite perfusion fixation with glutaraldehyde. A 10x objective (EC Plan-Neofluar 10x/0.30 M27) was used with an image matrix of 1024x1024 pixel, a pixel scaling of 0.2x0.2 µm and a color depth of 8 bit. The scanned region of approximately 2x2 mm covered the whole cortical thickness of the lesion and perilesion area in order to generate overview maps for later correlation. Whole brain images were collected in z-stacks as tile scans with a slice-distance of 5 µm and a total range of 50 µm. Specific regions of interest including the microthrombi and sites of extravasation were collected in single plane using 25x magnification (objective: EC Plan-Neofluar 25x/0,8 Imm Korr DIC M27) with an image matrix of 1024x1024 pixel, a pixel scaling of 0.2 x 0.2 µm and a depth of 8 bit. After imaging for maximal 1 hour, the glass slide was immersed into a petri dish filled with 1x PBS. As soon as the tissue section was floating from the glass sandwich, it was transferred into fresh buffer for storage.

Embedding of vibratome sections for electron microscopy

The sections were stored in PBS at 4°C for up to one week until the start of the postembedding. For correlation, the confocal imaging plane was ideally parallel to the ultramicrotomy sectioning plane. The searchable volume in the axial dimension is predetermined by and restricted to the vibratome section thickness. Usually, heavy metal impregnation leads to bending of the section. In order to avoid this sample preparation artifact and minimize the lateral searchable area, we dissected a region of approximately 1.5x2 mm capturing the lesion and perilesion area under the binocular using fine scalpels. The fluorescence overview tile scan was used as a template to relocate the previously imaged region. The overall section shape, including big blood vessels and bleedings that represent non-fluorescent regions in the confocal template were used for this coarse lateral re-location. We applied a standard reduced osmium thiocarbohydrazide osmium (rOTO) *en bloc* staining protocol (Kislinger et al., 2020a [DOI](#)) including postfixation in 2% osmium tetroxide (EMS), 1.5% potassium ferrocyanide (Sigma) in 0.1 M sodium cacodylate (Science Services) buffer (pH 7.4). Staining was enhanced by reaction with 1% thiocarbohydrazide (Sigma) for 45 min at 40 °C. The tissue was washed in water and incubated in 2% aqueous osmium

tetroxide, washed and further contrasted by overnight incubation in 1% aqueous uranyl acetate at 4° C and 2h at 50° C. Samples were dehydrated in a graded series of ethanol and infiltrated with LX112 (LADD) resin.

Plastic tape coating

Initially, we coated ~10 cm long carbon-coated Kapton (ccKapton) (kindly provided by Jeff Lichtman and Richard Schalek) or carbon nanotube (Science Services) tape strips with 1 % (w/v) Formvar in chloroform (Sigma) using a standard film casting device for grids (Science Services). In order to generate a homogenous film on longer ccKapton tape pieces we designed a spray-coating device. This custom-built coating machine was equipped with a holder for the spraying unit (Lubrimat L60, Steidle) and two tape reels driven by a motor (Suppl. Fig. 1). However, this method proved to be unreliable, as the chloroform caused deterioration of the spraying unit over time which, in turn, lead to uneven and debris-contaminated coatings. Heterogeneous coating resulted in charging during or detachment problems after SEM imaging.

In order to enable section removal, we marked ccKapton tape on its coated side with a permanent marker (edding 3000, black, edding International GmbH, Germany). We used the before-mentioned coating machine and replaced the spraying unit by the permanent parker. Thereby, the marker was constantly pressed onto the tape as it was pulled under the marker tip to ensure uniform tape coating (**Fig. 2E** [↗](#)).

First, we treated ccKapton in a custom-built tape plasma discharger based on easiGlow (Pelco, negative polarity, 0.35 mBar, 15 mA) that we adopted from Mark Terasaki (U. Connecticut). After four runs at ~0.5 mm/s, the tape was wrapped around the glass insert of a standard plasma discharger (Harrick Plasma PDC-32C, air, setting “high”) for 1 min.

Section collection onto coated tape

For the volume analysis, the block was trimmed at a depth of 100 µm and a 45° angle on four sides using a trimming machine (EM TRIM, Leica). Serial sections were taken with a 35° ultra-maxi diamond knife (Diatome) at a nominal cutting thickness of 80-100 nm for ATUM-SEM and the TEM tests and 400 nm for ATUM-Tomo at the ATUMtome (Powertome, RMC). Sections were collected onto freshly plasma-treated, carbon nanotube tape (Science Services) for ATUM-SEM and either cpcKapton (carbon- and permanent marker coated) or cfcKapton (carbon- and Formvar-coated) for ATUM-Tomo. Covering the whole sample thickness of 80 µm and considering its unevenness after contrasting, either 1000 sections at 100 nm thickness (ATUM-SEM) or 400 sections at 400 nm thickness (ATUM-Tomo) were taken. Plastic tape stripes were assembled onto adhesive carbon tape (Science Services) attached to 4-inch silicon wafers (Siegert Wafer) and grounded by adhesive carbon tape strips (Science Services). For each sample, 4-6 (ATUM-SEM) or 1-2 (ATUM-Tomo) wafers each bearing 200-300 sections were generated.

Serial-section acquisition by SEM

ATUM-SEM was performed on a Crossbeam Gemini 340 SEM (Zeiss) with a four-quadrant backscatter detector at 8 kV. Hierarchical imaging captures large areas at low resolution that can, in turn, be screened for structures of interest that are subsequently reimaged at higher resolution and so forth. In ATLAS5 Array Tomography (Fibics), wafer overview images were generated (1000 nm/pixel). We acquired whole section low resolution images (0.1 x 0.1 x 1 µm) of every 10th section (thus simulating the thickness of one confocal plane covering 1 µm thickness) to generate overviews that can be correlated with the confocal imaging data. We used blood vessel patterns, bleedings and the different tissue layers as landmarks. Target regions were identified and acquired at medium resolution (20 x 20 x 200 nm). Within this volume, clots were selected for high-resolution imaging (4-20 x 4-20 x 200 nm).

For ATUM-Tomo, electron micrographs were acquired in a similar hierarchical scheme on an Apreo S2 SEM (Thermo Fisher Scientific) with the T1 detector. Serial-section acquisition was performed using the Maps2 (Thermo Fisher Scientific) software. We acquired images of whole sections at low resolution (100 x 100 x 400 nm) to facilitate re-location. Anatomical landmarks and vasculature patterns of single SEM overview images and a summed (in Fiji) stack of sections were compared to the confocal data sets in Fiji. Within this volume, we selected a region with clots and transition zones and extravasation for high-resolution imaging at 20 x 20 x 400 nm. We acquired subsets of these regions on each or every second section at 10 x 10 x 400 nm 10 x 10 x 800 nm resolution, respectively.

Correlation and volume image analysis

There were two levels of correlation: first, we dissected the tissue according to the field of view of confocal imaging and second, we identified occlusions of interest in the low-resolution SEM data for high-resolution imaging. At each step, anatomical landmarks (bleedings with accumulation of erythrocytes, the section outline etc.) and vasculature patterns of single and summed sections were compared to the confocal data sets in Fiji ([Schindelin et al., 2012](#)) or using the ec-CLEM ICY plugin ([Paul-Gilloteaux et al., 2017](#)). We used single and the sum (in Fiji) of a stack of SEM images for relocation of the occlusions of interest. Serial section data were aligned by a sequence of automatic and manual processing steps in Fiji TrakEM2 ([Kislinger et al., 2023](#)). The VAST software was used for manual segmentation of blood vessels ([Berger et al., 2018](#)) that were rendered in Blender ([Brito, 2018](#)) for better visualization.

Section retrieval from coated tape onto TEM grids

Based on SEM-imaging results and the corresponding three-dimensional SEM data, we selected sections of interest for subsequent TEM imaging. We cut the carbon adhesive tape around the selected section on the wafer using a scalpel and peeled off the section-containing piece of cpcKapton from the adhesive tape (**Fig. 2B,C**). Next, we submerged the piece of tape containing one single section of interest in a glass petri dish containing acetone. We then created a steady acetone flow with a plastic transfer pipette until the coating between tape and section was dissolved, resulting in a section floating in the acetone bath. In our experience, the required rinsing time increases with previous beam exposure of the section in the SEM. Once floating in the acetone bath, we collected the single section in a plastic transfer pipette and released it into a water-filled boat (as used for sectioning with diamond knives, kindly provided by Diatome). Through the surface tension of the water, the section stretched and floated on the water surface. However, through the detachment from the tape in the acetone bath, it could happen that the sections were physically reversed on the water bath relative to the sectioning direction.

TEM of ultrathin sections

Ultrathin sections were removed from cfcKapton or cpcKapton tape using chloroform or acetone. Retrieved sections were collected onto Formvar-coated copper grids (Science Services). Sections were imaged using a JEM-1400+ (JEOL) transmission electron microscope (TEM) equipped with a XF416 (TVIPS) camera operated by the EM-Menu software (TVIPS).

ET of semi-thick sections

For ET, single serial semi-thick (400 nm) sections were released as described above and collected on slot grids covered with a Formvar layer of golden interference color. Colloidal gold particles (diameter 20 nm, BBI) serving as fiducials for tomographic reconstruction were then attached to the sections by submerging the grids into a droplet of the pure colloidal gold solution for 1 min. Samples were blotted to remove residual solution and air-dried. Semi-thick sections were imaged using a Tecnai F30 transmission electron microscope (Thermo Fisher Scientific) operated at 300 kV and equipped with a 4k x 4k CMOS camera (OneView, Gatan) as previously described ([Kiewisz et al., 2022](#)). Using a dual-axis specimen holder (Type 2040, Fishione, USA), tilt series were

recorded from -60° to $+60^\circ$ with 1° increments at a magnification of 4700x and a pixel size of 2.572 nm applying the SerialEM software package (Mastronarde, 2003 [↗](#), Mastronarde, 2005 [↗](#)). For dual-tilt electron tomography, the grid was rotated for 90° in the XY-plane and the second tilt series was acquired using identical microscope settings (Mastronarde, 1997 [↗](#)). Both tomographic image stacks of the same positions were reconstructed, combined and flattened using IMOD (Kremer et al., 1996 [↗](#), Mastronarde and Held, 2017 [↗](#)). Serial semi-thick sections were stitched and combined by using the ZIB Amira (Zuse Institute Berlin, Germany) software package (Stalling et al., 2005 [↗](#), Lindow et al., 2021 [↗](#)). After converting the image data into TIFF format, the image registration was manually refined in Fiji TrakEM2., followed by a final elastic alignment. Segmentation of cellular features was performed manually with the program VAST (Berger et al., 2018 [↗](#)) and subsequently rendered in Blender (Brito, 2018 [↗](#)).

Acknowledgements

This work was supported by the DFG under Germany's Excellence Strategy within the framework of the Munich Cluster for Systems Neurology (SyNergy; EXC 2145 – ID 390857198), TRR 274/1 2020 (projects Z01 and B03 – ID 408885537) and FOR Immunostroke (Mi 694/9-1 A03 – ID 428663564). Research in the Müller-Reichert lab was funded by the DFG (grant MU 1423/8-2 to TMR). All animal experiments were supported by DFG grant 457586042. We thank Felix Beyer and Gero Finck (TUM, SyNergy NeuroCore), Dr. Tobias Fürstenhaupt (Electron microscopy lab at MPI-CBG, Dresden) for excellent technical assistance and Théo Cerciati (TUM) for segmentation.

Supplementary Data

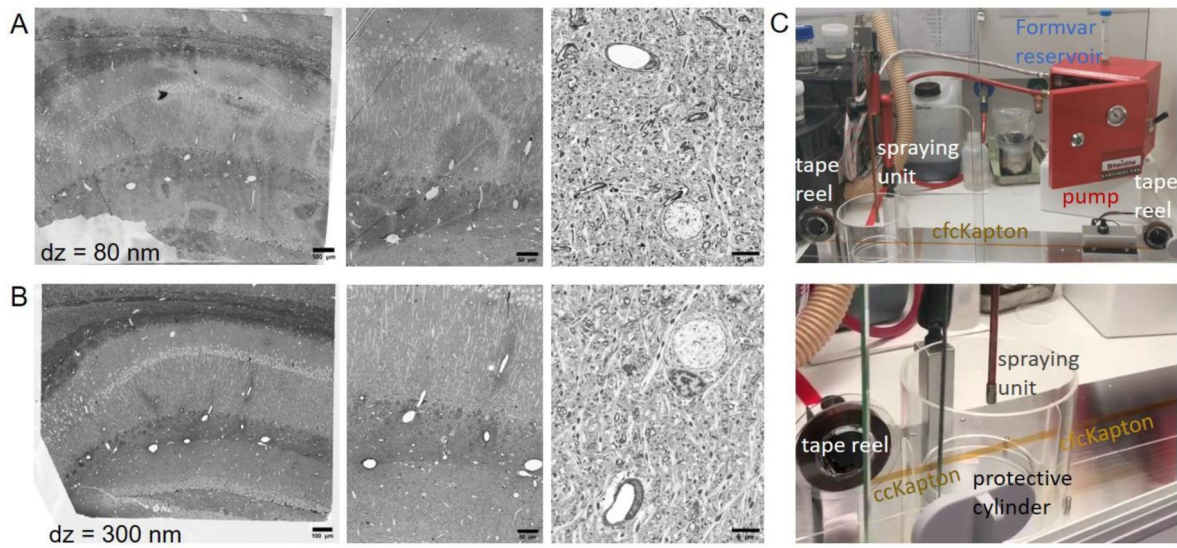


Figure 2 – Figure supplement 1.

Formvar coating for reversible section collection. Ultrathin (80 nm thickness) (A) and semi-thick (300 nm thickness) (B) sections imaged by SEM (BSD detector, 8 kV). From left to right: higher resolution and images. (A) Irregular Formvar coating can be detected on the first two images of ultrathin sections while (B) the semi-thick sections do not show any background originating from Formvar. High-resolution images of both ultra- and semi-thick sections are free of background from the coat. Scale bars 100 μm (left), 50 μm (middle), 5 μm (right). (C) Photos of the tape coating unit attached to a spraying unit (Lubrimat L60) for dispersion of Formvar onto the tape. Top: The red spraying unit with Formvar reservoir (Falcon tube) is shown as well as the reel-to-reel system for movement of the cckapton tape. Bottom: The spray nozzle dispersing the Formvar is surrounded by a Plexiglas cylinder that the tape can transverse.

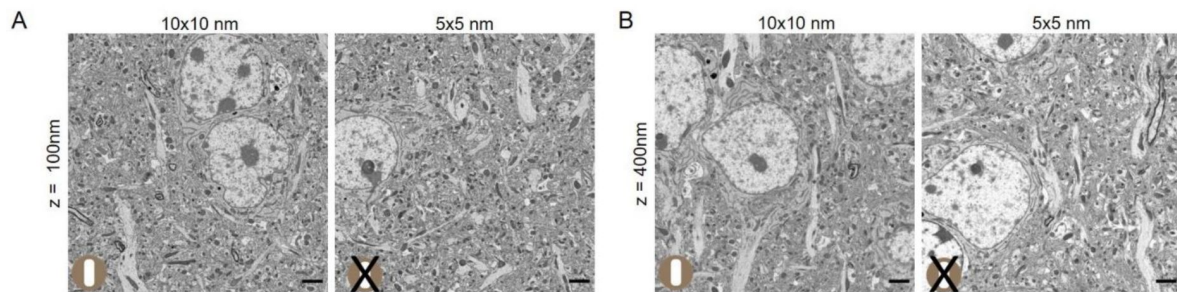


Figure 2 – Figure supplement 2.

Optimizing SEM imaging conditions for section detachment. (A) Ultrathin (100 nm thick) and (B) Semi-thick (400 nm thick) sections imaged at 10 nm (left) and 5 nm (right) lateral resolution at 5 kV, 4kV beam deceleration. Only sections imaged at 10 nm lateral resolution could be detached from cpcKapton after imaging, the ones imaged at 5 nm resolution were stuck to the tape. Scale bars 2 μm .

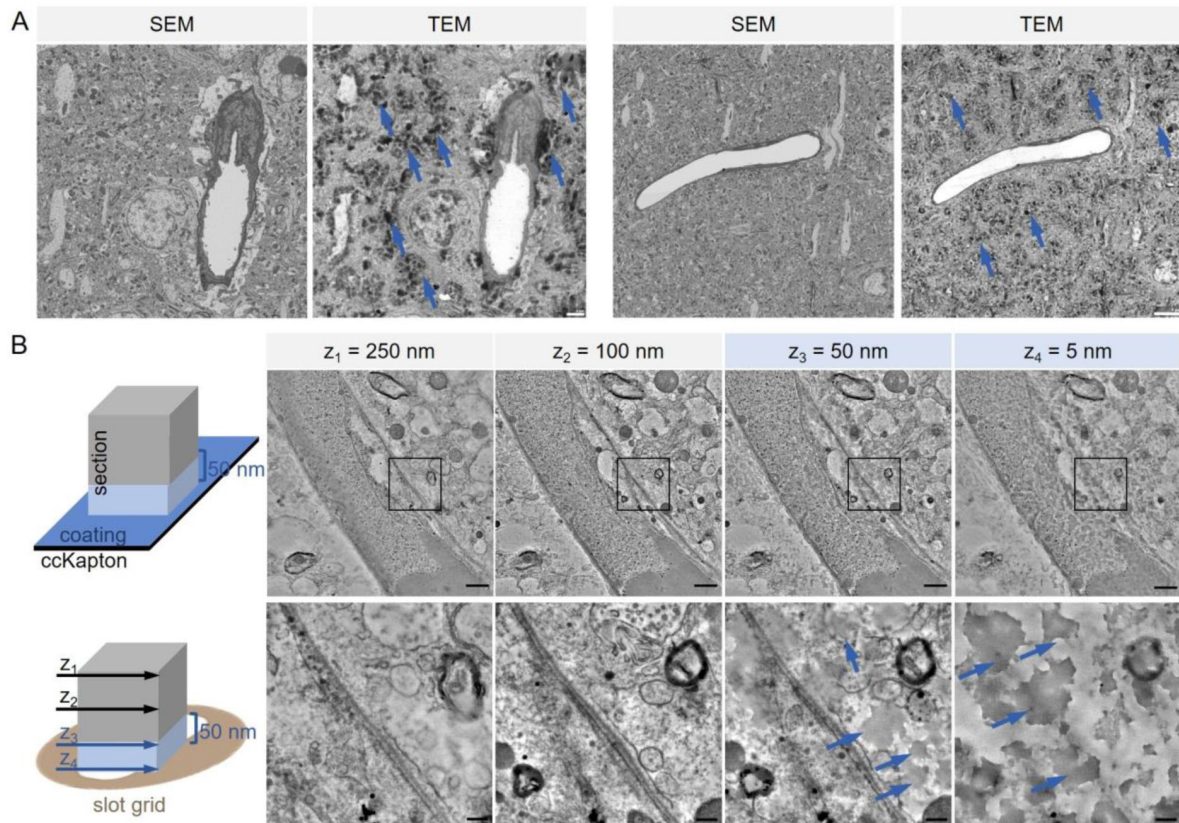


Figure 2 - Figure supplement 3.

Contamination of section surface after detachment. (A) Ultrathin sections imaged by SEM (left) and TEM (right). The TEM image shows contaminations (arrows). Scale bars 2 μ m (left), 5 μ m (right). (B) Scheme of the section attached to cKaptan (permanent marker coat, blue) and after collection onto a slot grid. The section side that faced the coating is contaminated (light blue) up to a thickness of 50 nm while the rest of the section thickness (grey) does not show any dirt originating from the coating. Single images of a tomographic reconstruction at different depths, indicated in the scheme (z_1 - z_4) are shown. The first left image (z_1) is superficial and the second is a middle one (z_2), both without dirt. The third image at 50 nm distance from the side that faced the coating (z_3) shows some dirt (arrow) while one of the images from the very bottom (z_4) is most contaminated. High magnification images (bottom) of the boxed regions reveal details of the contamination. Scale bars 1 μ m (top), 500 nm (bottom)

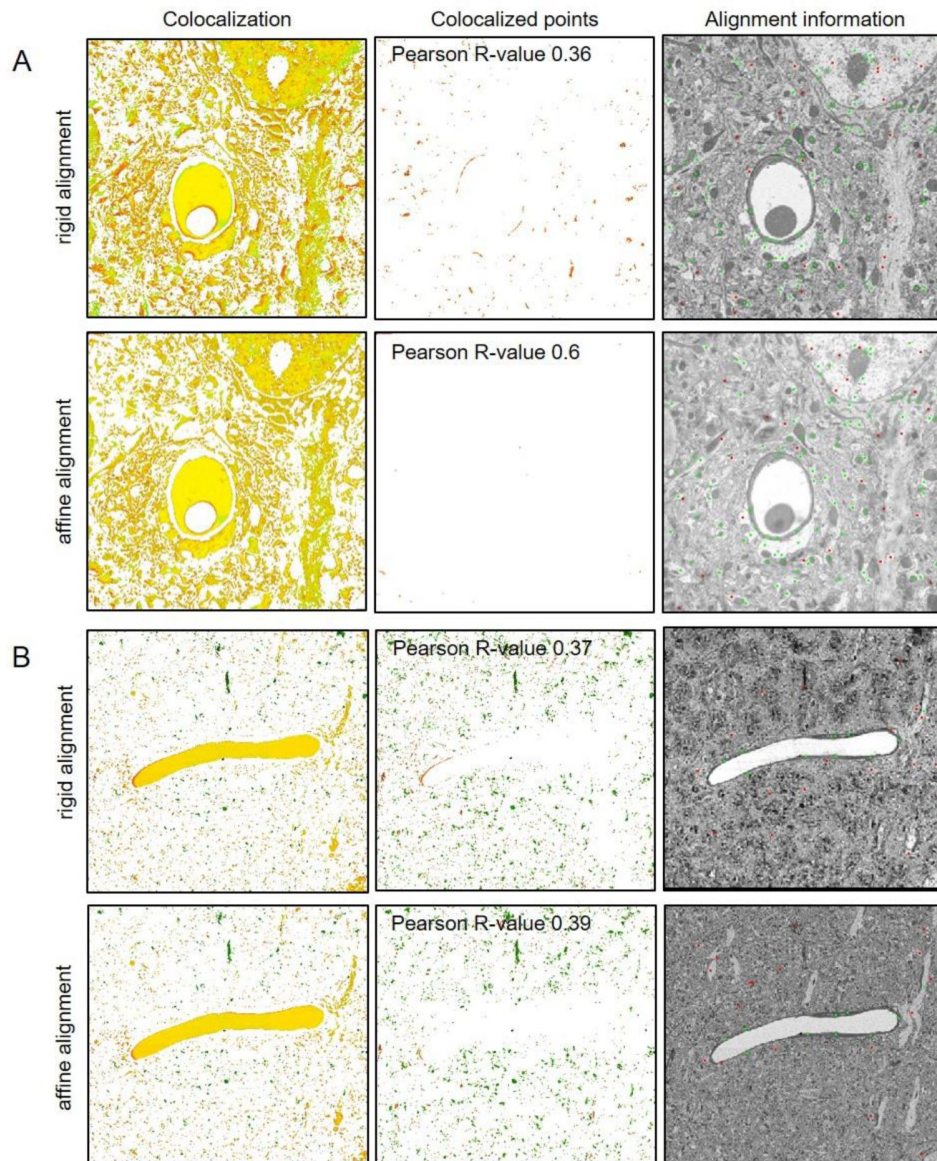


Figure 2 – Figure supplement 4.

Estimation of distortion between SEM and TEM images. Ultrathin section SEM and TEM images were compared after rigid (top) and affine (bottom) alignment to assess image distortion. We picked a clean example (A) and one region with some dirt (B). For both examples and alignment algorithms we calculated the Pearson coefficient between the SEM and TEM image. The images show the spatial distribution of colocalization (left, ImageJ 'Colocalization Finder') and mislocalization (middle, ImageJ 'Colocalization Highlighter'). The right images are calculated from the transformation of rigid to affine alignment (ImageJ 'Image Registration with SIFT'). Green indicates matching, red diverging points.

References

- Andreone B. J., Chow B. W., Tata A., Lacoste B., Ben-Zvi A., Bullock K., Deik A. A., Ginty D. D., Clish C. B., Gu C (2017) **Blood-Brain Barrier Permeability Is Regulated by Lipid Transport-Dependent Suppression of Caveolae-Mediated Transcytosis** *Neuron* **94**:581–594
- Baena V., Schalek R. L., Lichtman J. W., Terasaki M (2019) **Serial-section electron microscopy using automated tape-collecting ultramicrotome (ATUM)** *Methods Cell Biol* **152**:41–67
- Barth M., Bryan R. K., Hegerl R., Baumeister W (1988) **Estimation of missing cone data in three-dimensional electron microscopy** *Scanning Microsc Suppl* **2**:277–84
- Baumeister W., Grimm R., Walz J (1999) **Electron tomography of molecules and cells** *Trends in Cell Biology* **9**:81–85
- Berger D. R., Seung H. S., Lichtman J. W (2018) **VAST (Volume Annotation and Segmentation Tool): Efficient Manual and Semi-Automatic Labeling of Large 3D Image Stacks** *Front Neural Circuits* **12**
- Bouchaala R., Mercier L., Andreiuk B., Mély Y., Vandamme T., Anton N., Goetz J. G., Klymchenko A. S (2016) **Integrity of lipid nanocarriers in bloodstream and tumor quantified by near-infrared ratiometric FRET imaging in living mice** *J Control Release* **236**:57–67
- Brito A (2018) **Blender Quick Start Guide: 3D Modeling, Animation, and Render with Eevee in Blender 2.8**
- Ding G., Liu Y., Zhang R., Xin H. (2019) **'A joint deep learning model to recover information and reduce artifacts in missing-wedge sinograms for electron tomography and beyond'** *Scientific Reports* **9**:1–13
- Feng D., Nagy J. A., Dvorak H. F., Dvorak A. M (2002) **Ultrastructural studies define soluble macromolecular, particulate, and cellular transendothelial cell pathways in venules, lymphatic vessels, and tumor-associated microvessels in man and animals** *Microscopy Research and Technique* **57**:289–326
- Frank J (1970) **'Electron tomography : methods for three-dimensional visualization of structures in the cell'**
- 11 Ghosh M., Balbi M., Hellal F., Dichgans M., Lindauer U., Plesnila N. (2015) **'Pericytes are involved in the pathogenesis of cerebral autosomal dominant arteriopathy with subcortical infarcts and leukoencephalopathy'** *Ann Neurol* **78**:887–900
- Graham B. J., Hildebrand D. G. C., Kuan A. T., Maniates-Selvin J. T., Thomas L. A., Shanny B. L., Lee W.-C. A (2019) **High-throughput transmission electron microscopy with automated serial sectioning** *bioRxiv* **657346**
- Guillen J (2012) **FELASA guidelines and recommendations** *J Am Assoc Lab Anim Sci* **51**:311–21
- Hayworth K. J., Xu C. S., Lu Z., Knott G. W., Fetter R. D., Tapia J. C., Lichtman J. W., Hess H. F (2015) **Ultrastructurally smooth thick partitioning and volume stitching for large-scale connectomics** *Nature Methods* **12**:319–322

He W., He Y (2014) **Electron tomography for organelles, cells, and tissues** *Methods Mol Biol* **1117**:445–83

Hirano A., Kawanami T., Llena J. F (1994) **Electron microscopy of the blood-brain barrier in disease** *Microscopy Research and Technique* **27**:543–556

Holler S., Köstinger G., Martin K. A. C., Schuhknecht G. F. P., Stratford K. J (2021) **Structure and function of a neocortical synapse** *Nature* **591**:111–116

Horstmann H., Körber C., Sätzler K., Aydin D., Kuner T (2012) **Serial Section Scanning Electron Microscopy (S3EM) on Silicon Wafers for Ultra-Structural Volume Imaging of Cells and Tissues** *PLOS ONE* **7**

Hua Y., Laserstein P., Helmstaedter M (2015) **Large-volume en-bloc staining for electron microscopy-based connectomics** *Nature Communications* **6**

Karreman M. A., Ruthensteiner B., Mercier L., Schieber N. L., Solecki G., Winkler F., Goetz J. G., Schwab Y, Müller-Reichert T., Verkade P (2017) **'Chapter 13 - Find your way with X-Ray: Using microCT to correlate in vivo imaging with 3D electron microscopy'** :277–301

Kasthuri N., Hayworth Kenneth J., Berger Daniel R., Schalek Richard L., Conchello José A., Knowles-Barley S., Lee D., Vázquez-Reina A., Kaynig V., Jones Thouis R., Roberts M., Morgan Josh L., Tapia Juan C., Seung H. S., Roncal William G., Vogelstein Joshua T., Burns R., Sussman Daniel L., Priebe Carey E., Pfister H., Lichtman Jeff W (2015) **Saturated Reconstruction of a Volume of Neocortex** *Cell* **162**:648–661

Khalin I., Adarsh N., Schifferer M., Wehn A., Groschup B., Misgeld T., Klymchenko A., Plesnila N (2022) **Size-Selective Transfer of Lipid Nanoparticle-Based Drug Carriers Across the Blood Brain Barrier Via Vascular Occlusions Following Traumatic Brain Injury** *Small, n/a(n/a)* **2200302**

Khalin I., Heimburger D., Melnychuk N., Collot M., Groschup B., Hellal F., Reisch A., Plesnila N., Klymchenko A. S (2020) **Ultrabright Fluorescent Polymeric Nanoparticles with a Stealth Pluronic Shell for Live Tracking in the Mouse Brain** *ACS Nano* **14**:9755–9770

Kiewisz R., Fabig G., Conway W., Baum D., Needleman D., Müller-Reichert T (2022) **Three-dimensional structure of kinetochore-fibers in human mitotic spindles** *eLife* **11**

Kilkenny C., Browne W. J., Cuthill I. C., Emerson M., Altman D. G (2010) **Improving Bioscience Research Reporting: The ARRIVE Guidelines for Reporting Animal Research** *PLOS Biology* **8**

Kislinger G., Gnägi H., Kerschensteiner M., Simons M., Misgeld T., Schifferer M (2020) **ATUM-FIB microscopy for targeting and multiscale imaging of rare events in mouse cortex** *STAR Protocols* **1**

Kislinger G., Gnägi H., Kerschensteiner M., Simons M., Misgeld T., Schifferer M. (2020) **'Multiscale ATUM-FIB Microscopy Enables Targeted Ultrastructural Analysis at Isotropic Resolution'** *iScience* **23**

Kislinger G., Niemann C., Rodriguez L., Jiang H., Fard M. K., Snaidero N., Schumacher A.-M., Kerschensteiner M., Misgeld T., Schifferer M (2023) **'Neurons on tape: Automated Tape Collecting Ultramicrotomy-mediated volume EM for targeting neuropathology'**

Knowland D., Arac A., Sekiguchi Kohei J., Hsu M., Lutz Sarah E., Perrino J., Steinberg Gary K., Barres Ben A., Nimmerjahn A., Agalliu D (2014) **Stepwise Recruitment of Transcellular and Paracellular Pathways Underlies Blood-Brain Barrier Breakdown in Stroke** *Neuron* **82**:603–617

Kremer J. R., Mastronarde D. N., McIntosh J. R (1996) **Computer visualization of three-dimensional image data using IMOD** *J Struct Biol* **116**:71–6

Krueger M., Bechmann I., Immig K., Reichenbach A., Härtig W., Michalski D (2015) **Blood-brain barrier breakdown involves four distinct stages of vascular damage in various models of experimental focal cerebral ischemia** *J Cereb Blood Flow Metab* **35**:292–303

Krueger M., Mages B., Hobusch C., Michalski D (2019) **Endothelial edema precedes blood-brain barrier breakdown in early time points after experimental focal cerebral ischemia** *Acta Neuropathologica Communications* **7**

Kubota Y., Sohn J., Hatada S., Schurr M., Straehle J., Gour A., Neujahr R., Miki T., Mikula S., Kawaguchi Y (2018) **A carbon nanotube tape for serial-section electron microscopy of brain ultrastructure** *Nature Communications* **9**

Lindow N., Brünig F. N., Dercksen V. J., Fabig G., Kiewisz R., Redemann S., Müller-Reichert T., Prohaska S., Baum D (2021) **Semi-automatic stitching of filamentous structures in image stacks from serial-section electron tomography** *J Microsc* **284**:25–44

Luther P. K., Lawrence M. C., Crowther R. A (1988) **A method for monitoring the collapse of plastic sections as a function of electron dose** *Ultramicroscopy* **24**:7–18

Maniates-Selvin J. T., Hildebrand D. G. C., Graham B. J., Kuan A. T., Thomas L. A., Nguyen T., Buhmann J., Azevedo A. W., Shanny B. L., Funke J., Tuthill J. C., Lee W.-C. A. (2020) **'Reconstruction of motor control circuits in adult *Drosophila* using automated transmission electron microscopy'** *bioRxiv*

Mastronarde D. N (1997) **Dual-axis tomography: an approach with alignment methods that preserve resolution** *J Struct Biol* **120**:343–52

Mastronarde D. N (2003) **SerialEM: A Program for Automated Tilt Series Acquisition on Tecnai Microscopes Using Prediction of Specimen Position** *Microscopy and Microanalysis* **9**:1182–1183

Mastronarde D. N (2005) **Automated electron microscope tomography using robust prediction of specimen movements** *J Struct Biol* **152**:36–51

Mastronarde D. N., Held S. R (2017) **Automated tilt series alignment and tomographic reconstruction in IMOD** *J Struct Biol* **197**:102–113

McEwen B. F., Marko M, Rieder C.L (1998) **'Chapter 5 Three-Dimensional Transmission Electron Microscopy and Its Application to Mitosis Research'** :81–111

Michel C. C (2012) **Electron Tomography of Vesicles** *Microcirculation* **19**:473–476

Micheva K. D., Smith S. J (2007) **Array Tomography: A New Tool for Imaging the Molecular Architecture and Ultrastructure of Neural Circuits** *Neuron* **55**:25–36

- Nahirney P. C., Reeson P., Brown C. E (2016) **Ultrastructural analysis of blood-brain barrier breakdown in the peri-infarct zone in young adult and aged mice** *Journal of cerebral blood flow and metabolism : official journal of the International Society of Cerebral Blood Flow and Metabolism* **36**:413–425
- O’Brown N. M., Megason S. G., Gu C. (2019) **Suppression of transcytosis regulates zebrafish blood-brain barrier function** *eLife* **8**
- O’Toole E., Morphew M., McIntosh J. R. (2020) **Electron tomography reveals aspects of spindle structure important for mechanical stability at metaphase** *Mol Biol Cell* **31**:184–195
- Paez-Segala M. G., Sun M. G., Shtengel G., Viswanathan S., Baird M. A., Macklin J. J., Patel R., Allen J. R., Howe E. S., Piszczek G., Hess H. F., Davidson M. W., Wang Y., Looger L. L (2015) **Fixation-resistant photoactivatable fluorescent proteins for CLEM** *Nature methods* **12**:215–218
- Paul-Gilloteaux P., Heiligenstein X., Belle M., Domart M.-C., Larijani B., Collinson L., Raposo G., Salamero J (2017) **eC-CLEM: flexible multidimensional registration software for correlative microscopies** *Nature Methods* **14**:102–103
- Peddie C. J., Genoud C., Kreshuk A., Meechan K., Micheva K. D., Narayan K., Pape C., Parton R. G., Schieber N. L., Schwab Y., Titze B., Verkade P., Weigel A., Collinson L. M (2022) **Volume electron microscopy** *Nature Reviews Methods Primers* **2**
- Pelchen-Matthews A., Marsh M (2007) **Electron microscopy analysis of viral morphogenesis** *Methods Cell Biol* **79**:515–42
- Rachel R., Heinz V., Flechsler J., Witzgall R., Heimerl T (2016) **Serial section (S)TEM tomography of prokaryotic cells** *European Microscopy Congress* :101–102
- Reisch A., Didier P., Richert L., Oncul S., Arntz Y., Mély Y., Klymchenko A. S (2014) **Collective fluorescence switching of counterion-assembled dyes in polymer nanoparticles** *Nature Communications* **5**
- Roingeard P (2008) **Viral detection by electron microscopy: past, present and future** *Biol Cell* **100**:491–501
- Scher N., Avinoam O (2021) **50 Shades of CLEM: How to choose the right approach for you** *Methods Cell Biol* **162**:1–11
- Schiffner M., Snaidero N., Djannatian M., Kerschensteiner M., Misgeld T (2021) **Niwaki Instead of Random Forests: Targeted Serial Sectioning Scanning Electron Microscopy With Reimaging Capabilities for Exploring Central Nervous System Cell Biology and Pathology** *Front Neuroanat* **15**
- Schindelin J., Arganda-Carreras I., Frise E., Kaynig V., Longair M., Pietzsch T., Preibisch S., Rueden C., Saalfeld S., Schmid B., Tinevez J.-Y., White D. J., Hartenstein V., Eliceiri K., Tomancak P., Cardona A (2012) **Fiji: an open-source platform for biological-image analysis** *Nature Methods* **9**:676–682
- Schneider J., Hegermann J., Wrede C (2021) **Volume electron microscopy: analyzing the lung** *Histochemistry and cell biology* **155**

Shi Y., Thrippleton M. J., Blair G. W., Dickie D. A., Marshall I., Hamilton I., Doubal F. N., Chappell F., Wardlaw J. M (2020) **Small vessel disease is associated with altered cerebrovascular pulsatility but not resting cerebral blood flow** *J Cereb Blood Flow Metab* **40**:85–99

Snaidero N., Schifferer M., Mezydło A., Zalc B., Kerschensteiner M., Misgeld T (2020) **Myelin replacement triggered by single-cell demyelination in mouse cortex** *Nature Communications* **11**

Soto G. E., Young S. J., Martone M. E., Deerinck T. J., Lamont S., Carragher B. O., Hama K., Ellisman M. H (1994) **Serial section electron tomography: a method for three-dimensional reconstruction of large structures** *Neuroimage* **1**:230–43

Stalling D., Westerhoff M., Hege H.-C., Hansen C., Johnson C. (2005) **Amira: A highly interactive system for visual data analysis** *The Visualization Handbook*

Wacker I., Schroeder R. R (2013) **Array tomography** *Journal of Microscopy* **252**:93–99

Wagner R., Modla S., Hossler F., Czymmek K (2012) **Three-Dimensional Analysis and Computer Modeling of the Capillary Endothelial Vesicular System with Electron Tomography** *Microcirculation* **19**:477–484

Wehn A. C., Khalin I., Duering M., Hellal F., Culmsee C., Vandenabeele P., Plesnila N., Terpolilli N. A (2021) **RIPK1 or RIPK3 deletion prevents progressive neuronal cell death and improves memory function after traumatic brain injury** *Acta Neuropathologica Communications* **9**

West M., Zurek N., Hoenger A., Voeltz G. K (2011) **A 3D analysis of yeast ER structure reveals how ER domains are organized by membrane curvature** *J Cell Biol* **193**:333–46

Wu H., Fujioka Y., Sakaguchi S., Suzuki Y., Nakano T (2022) **Three-dimensional reconstruction by electron tomography for the application to ultrastructural analysis of SARS-CoV-2 particles** *Medical Molecular Morphology* **55**:60–67

Yin W., Brittain D., Borseth J., Scott M. E., Williams D., Perkins J., Own C. S., Murfitt M., Torres R. M., Kapner D., Mahalingam G., Bleckert A., Castelli D., Reid D., Lee W. A., Graham B. J., Takeno M., Bumbarger D. J., Farrell C., Reid R. C., da Costa N. M (2020) **A petascale automated imaging pipeline for mapping neuronal circuits with high-throughput transmission electron microscopy** *Nat Commun* **11**

Young L. N., Villa E (2023) **Bringing Structure to Cell Biology with Cryo-Electron Tomography** *Annu Rev Biophys* **52**:573–595

Zhang H., Jin B., Faber J. E (2019) **'Mouse models of Alzheimer's disease cause rarefaction of pial collaterals and increased severity of ischemic stroke'** *Angiogenesis* **22**:263–279

70 Zhu J., Li Z., Ji Z., Wu Y., He Y., Liu K., Chang Y., Peng Y., Lin Z., Wang S., Wang D., Huang K., Pan S (2022) **Glycocalyx is critical for blood-brain barrier integrity by suppressing caveolin1-dependent endothelial transcytosis following ischemic stroke** *Brain Pathology* **32**

Article and author information

Georg Kislinger

Institute of Neuronal Cell Biology, Technical University Munich, Munich, Germany, German Center for Neurodegenerative Diseases (DZNE), Munich, Germany

Gunar Fabig

Experimental Center, Faculty of Medicine Carl Gustav Carus, Technische Universität Dresden, Dresden, Germany

Antonia Wehn

Institute for Stroke and Dementia Research (ISD), LMU University Hospital, LMU Munich, Germany, Department of Neurosurgery, University of Munich Medical Center, Munich, Germany

Lucia Rodriguez

Institute of Neuronal Cell Biology, Technical University Munich, Munich, Germany, German Center for Neurodegenerative Diseases (DZNE), Munich, Germany

Hanyi Jiang

Institute of Neuronal Cell Biology, Technical University Munich, Munich, Germany, German Center for Neurodegenerative Diseases (DZNE), Munich, Germany, Department of Psychiatry and Psychotherapy, University Medicine Greifswald, Greifswald, Germany

Cornelia Niemann

Institute of Neuronal Cell Biology, Technical University Munich, Munich, Germany, German Center for Neurodegenerative Diseases (DZNE), Munich, Germany

Andrey S. Klymchenko

Laboratoire de Biophotonique et Pharmacologie, CNRS UMR 7213, Université de Strasbourg, Illkirch, France

Nikolaus Plesnila

Institute for Stroke and Dementia Research (ISD), LMU University Hospital, LMU Munich, Germany, Munich Cluster of Systems Neurology (SyNergy), Munich, Germany

Thomas Misgeld

Institute of Neuronal Cell Biology, Technical University Munich, Munich, Germany, German Center for Neurodegenerative Diseases (DZNE), Munich, Germany, Munich Cluster of Systems Neurology (SyNergy), Munich, Germany

Thomas Müller-Reichert

Experimental Center, Faculty of Medicine Carl Gustav Carus, Technische Universität Dresden, Dresden, Germany

Igor Khalin

Institute for Stroke and Dementia Research (ISD), LMU University Hospital, LMU Munich, Germany

Martina Schifferer

German Center for Neurodegenerative Diseases (DZNE), Munich, Germany, Munich Cluster of Systems Neurology (SyNergy), Munich, Germany

For correspondence: martina.schifferer@dzne.de

Copyright

© 2023, Kislinger et al.

This article is distributed under the terms of the [Creative Commons Attribution License \(https://creativecommons.org/licenses/by/4.0/\)](https://creativecommons.org/licenses/by/4.0/), which permits unrestricted use and redistribution provided that the original author and source are credited.

Editors

Reviewing Editor

Nils Brose

Max Planck Institute of Experimental Medicine, Germany

Senior Editor

Albert Cardona

University of Cambridge, United Kingdom

Reviewer #1 Public Review**Summary**

This paper presents a new, but simple and low-cost technique for multimodal EM imaging that combines the strengths of both volume scanning electron microscopy (SEM) and electron microscopic tomography. The novel ATUM-Tomo approach enables the consecutive inspection of selected areas of interest by correlated serial SEM and TEM, optionally in combination with CLEM, as demonstrated here. The most important feature of ATUM-Tomo, particularly of correlative ATUM-Tomo, is that it can bridge scales, from the cellular to the high-resolution subcellular scale, from micrometer to low nanometer resolution. This is particularly important for ultrastructural analyses of biological regions of interest, which is demonstrated here for focal pathologies or rare cellular and subcellular events. Both imaging modalities are non-destructive, thus allowing re-imaging and hierarchical imaging at the SEM and TEM levels. This is particularly important for precious samples, including human biopsies and samples from complex CLEM experiments. Beyond the demonstrated neuropathology-related application, further use in investigating normal and pathologically altered brains, including human brain tissue samples that require high-resolution SEM and TEM in combination with immunohistochemistry, and virus or tracer injections, would be possible. Thus, ATUM-Tomo provides new possibilities in multimodal volume EM imaging for diverse areas of biological research.

Strengths

This paper is a very nice piece of work, bringing together modern high-end state-of-the-art technology that will allow us to investigate diverse biological questions in different areas of interest and at different scales. The paper is clear and well-written, although some additions are necessary to the methods section and the scientific results as exemplified by investigations of the blood-brain barrier. The discussion would benefit from an expansion of the part dealing with the scientific results. The paper is accompanied by excellent figures, supplemental information, and colored 3D-reconstructions, which makes it easy for the

reader to follow the experimental procedure and the scientific context. The authors may consider moving the supplemental figures into the main body of the paper, which would then still contain 'only' eight figures.

Weaknesses

There is some imbalance between the description of the state-of-the-art methodology and the scientific context.

Reviewer #2 Public Review

Summary

Kislinger et al. present a method permitting a targeted, multiscale ultrastructural imaging approach to bridge the resolution gap between large-scale scanning electron microscopy (SEM) and transmission electron microscopy (TEM). The key methodological development consists of an approach to recover sections of resin-embedded material produced by Automated Tape Collecting Ultramicrotomy (ATUM), thereby permitting regions of interest identified by serial section SEM (ATUM-SEM) screening to be subsequently re-examined at higher resolution by TEM tomography (ATUM-Tomo). The study shows that both formvar and permanent marker coatings are in principle compatible with the solvent-based release of pre-screened sections from ATUM tape (carbon nanotubule or Kapton tape). However, a comparative analysis of potential limitations and artifacts introduced by these respective coatings revealed permanent marker to provide a superior coating; permanent marker coatings are more easily and reliably applied to tape with only minor contaminants affecting the recovered section-tape interface with negligible influence on tomogram interpretation. Proof-of-principle is provided by integrating this novel ATUMTomo technique into a technically impressive correlated light and electron microscopy (CLEM) approach specifically tailored to investigate ultrastructural manifestations of trauma-induced changes in blood-brain barrier permeability (Khalin et al., 2022).

Strengths

Schematics and well-constructed figures clearly illustrate the general workflow, light and electron microscope image data are of excellent quality, and the efficacy of the ATUM-Tomo approach is documented by qualitative assessment of ATUM-SEM performance using coated tape variants and a convincing correlation between scanning and transmission electron microscopy imaging modalities. Potential ultrastructural artifacts induced via solvent exposure and any subsequent mechanical stress incurred during section detachment were systematically investigated using appropriate methods and transparently reported. In summary, the presented data are consistent with the study's claims. A major strength of this work includes its general applicability to a broad range of biological questions and ultrastructural targets demanding resolutions exceeding that obtained via serial section and block-face imaging approaches alone. Importantly, this relatively simple and cost-effective technique is widely adopted by electron microscopy laboratories. Its integration into existing ATUM-SEM workflows supports a versatile and non-destructive imaging regime enabling high-resolution details of targeted structures to be interpreted within anatomical and subcellular contexts.

Weaknesses

Given the identified importance of glow-discharge treatment of precoated tape to the flat deposition of sections during ATUM, a corresponding schematic or appropriate reference(s) providing more information about the custom-built tape plasma device would likely be a prerequisite for effective reproduction of this technique in other laboratories.

Author Response

We thank the Editors and Reviewers for the thorough assessment of our work. We are pleased that you agree with us that our proof-of-concept study of the ATUM Tomo technology advances volume electron microscopy and has the potential to solve research questions in diverse biological areas. Based on your comments, we are planning to revise the manuscript to optimize readability, clarify the fields of applicability of our approach more, and add some data related to questions you raised. We plan the following revisions:

Reviewer #1 The authors may consider moving the supplemental figures into the main body of the paper since they finally would end up with a total of eight figures.

As part of the supplemental figures describe essential experimental details, we will move them into the main part of the manuscript.

Reviewer #1 In general, the methods and techniques used here are beside some required but important additions described in sufficient detail.

Reviewer #2 Given the identified importance of glow-discharge treatment of precoated tape to the flat deposition of sections during ATUM, a corresponding schematic or appropriate reference(s) providing more information about the custom-built tape plasma device would likely be a prerequisite for effective reproduction of this technique in other laboratories.

Thank you for the valuable comments on the missing experimental details, which could affect the ease of establishing ATUM-Tomo in other labs. We will clearly highlight the ATUM-Tomo-specific vs. some general EM processing steps of the workflow in the proposed way. A detailed description of the custom-built tape plasma device will be added to the methods section. In addition, we will reference more explicitly our published protocols, which describe the standard electron microscopy embedding steps in great detail (Kislinger et al., STAR protocols, 2020; Kislinger et al., Meth Cell Biol, 2023).

Reviewer #1 Concerning the results section: In my opinion, the results section is a bit unbalanced. There is a mismatch between the detailed description of the methodology (experimental approach) and the scientific findings of the paper. The reviewer can see the enormous methodological impact of the paper, which on the other hand is the major drawback of the paper. To my opinion, the authors should also give a more detailed description of their scientific results.

Concerning the discussion: It would have been nice to give a perspective to which the described methodology can be used not only to describe diverse biological aspects that can be addressed and answered by this experimental approach. For example, how could this method be used to address various questions about the normal and pathologically altered brain?

In my opinion, the paper has one major drawback which is that it is more methodologically based although the authors included a scientific application of the method. The question here is to balance the methodology vs. the scientific achievement of this paper, a decision hard to take. In other words, one could recommend this paper to more methodologically based journals, for example, Nature Methods.

Balancing the technological and biological parts is indeed a difficult issue. We agree that this manuscript mainly describes a technical advancement and demonstrates its power to answer previously unsolved scientific questions. We exemplify this in our model system, neuropathology of the blood-brain barrier. The biological impact of ATUM-SEM has been

described in detail in Khalin et al., Small, 2022, and is referenced accordingly. Here we describe how ATUM-Tomo can be applied to reveal biological insights exceeding the capabilities of ATUM-SEM and other volume electron microscopy techniques. However, the description of the methodological development outweighs by far the one of the biological details. We consider eLife's Tools and Resources (which, in our view, is in scope similar to Nat Methods) an ideal format for this technically focused manuscript while targeting eLife's readership with diverse biological fields of interest for potential applications of the method. We will add more suggestions for possible applications to the discussion to accommodate the Reviewer's concern that having only a single application might seem arbitrary or even suggest a very narrow utility of the technique.

Reviewer #2 Is the separation of sections from permanent marker-treated tape sensitive to the time interval between deposition/SEM imaging and acetone treatment?

Thank you for pointing out this important methodological aspect. We have not systematically investigated whether there is a critical time window between microtomy, SEM, and detachment. From the samples generated for this study, we will try to assess the importance of timing in retrospect.

Reviewer #2 To what extent is slice detachment from permanent marker-treated tape resin-dependent [i.e. has ATUM-Tomo been tested on resin compositions beyond LX112 (LADD)]?

We appreciate this comment addressing the broader technical applicability of ATUM-Tomo. We aim to test the general workflow with tissue embedded in other commonly used resin types.

Reviewer #2 Minor corrections to the text and figures.

Thank you for the detailed corrections. We will apply them accordingly.